Clays and Clay Minerals, Vol. 63, No. 2, 132–143, 2015.

KEY STEPS INFLUENCING THE FORMATION OF ALUMINOSILICATE NANOTUBES BY THE FLUORIDE ROUTE

ATIKA CHEMMI, JOCELYNE BRENDLE*, CLAIRE MARICHAL, AND BENEDICTE LEBEAU

Pôle Matériaux à Porosité Contrôlée (MPC), Institut de Science des Matériaux de Mulhouse (IS2M), CNRS UMR 7361, Université de Haute Alsace (UHA), ENSCMu, 3b rue Alfred Werner 68093 Mulhouse Cedex, France

Abstract—Imogolite is usually formed by means of a three-step process involving the use of large amounts of water with long crystallization times and low yields, preventing large-scale synthesis. These drawbacks can be overcome by synthesis in the presence of fluoride, an approach which has been demonstrated to be suitable for the synthesis of other phyllosilicates. In the present study, the nature of the Al and Si sources, the Al/Si molar ratio, the volume of H_2O for the redispersion of the gel after desalination, the F/Si molar ratio, as well as the crystallization temperature and time have been varied to investigate their role in the crystallization of imogolite. The structural properties of the as-synthesized samples were characterized by X-ray diffraction, infrared spectroscopy, and ^{29}Si, ^{27}Al, and ^{19}F magic angle spinning nuclear magnetic resonance spectroscopy. The results show that the imogolite nanotubes can be prepared with high yields (>55%) from $AlCl_3{\cdot}6H_2O$ and Na_4SiO_4 aqueous solutions with an Al/Si molar ratio of 2.5, addition of HF for a F/Si molar ratio of 0.1−0.2, and 4 days of crystallization at 98ºC.

Key Words—Aluminosilicate Nanotube, Fluoride Route, Imogolite.

INTRODUCTION

Imogolite nanotubes were first discovered in 1962 in volcanic soils (Yoshinaga and Aomine, 1962) and have generated considerable interest amongst those working in nanotechnology research. Their well defined composition, size, morphology, nanoscale dimensions (Farmer, 1983), porosity (Adams, 1980; Ackerman *et al.*, 1993), hydrophilic surface (Gustafsson, 2001), and ability to be functionalized (Johnson and Pinnavaia, 1990; Jiravanichanun *et al.*, 2009; Ma *et al.*, 2011) enable a wide range of applications in catalysis (Imamura *et al.*, 1996), gas storage (Ackerman *et al.*, 1993), adsorption (Wilson *et al.* 2001; Clark, 1984; Zanzottera *et al.*, 2012), and heat exchange (Theng *et al.*, 1982).

Imogolite is a poorly crystalline hydrated aluminosilicate forming a single-walled nanotube with an outer diameter of 2 nm, an inner diameter of 1 nm, and a length of several micrometers. The tube wall is composed of a curved gibbsite ($Al(OH)_3$) layer on the outer surface and silicate tetrahedra linked to six aluminum octahedra inside the tube. The empirical formula of imogolite is $(HO)_3Al_2O_3SiOH$. Several protocols for the synthesis of imogolite have been reported in the literature (Farmer *et al.*, 1977; Wada *et al.*, 1979; Levard *et al.*, 2009; Yucelen *et al.*, 2011). Generally the established synthesis processes can be divided into three steps in which carefully controlled experimental conditions are required. The first step consists of the hydrolysis of inorganic Al and Si sources using NaOH which leads to the formation of the imogolite precursor, namely proto-imogolite. The use of several Al sources such as $Al(ClO_4)_3$ (Levard *et al.*, 2008), $AlCl_3{\cdot}6H_2O$ (Thomas *et al.*, 2012), $Al(NO_3)_3{\cdot}9H_2O$ (Bishop *et al.*, 2013), or $Al(C_4H_3O)_3$ (Denaix *et al.*, 1999) has been reported in the literature. Among these sources, $Al(ClO_4)_3$ or $AlCl_3{\cdot}6H_2O$ are most commonly employed. Perchlorates are preferred to chlorides because of their lower complexing ability, reducing the formation of by-products such as boehmite or amorphous silica (Mukherjee *et al.*, 2007; Thomas *et al.*, 2012). Tetraethylorthosilicate (TEOS) (Mukherjee *et al.*, 2005), Na_4SiO_4 (Ohashi *et al.*, 2004), fused sodium silicate (Hu *et al.*, 2004), or rice-husk ash (Hongo *et al.*, 2013) are used as silicon sources. The TEOS is usually preferred because of its slower condensation kinetics. The second step consists of adjusting the pH in the range 4.5−5 by addition of an acid solution such as HCl or a mixture of acids such as HCl and CH_3COOH (Barrett *et al.*, 1991; Yamamoto *et al.*, 2002). Finally, during the third step, crystallization of imogolite nanotubes occurs upon heating at 100ºC. Several parameters are involved in these three steps that control the formation of imogolite. They can be divided into chemical factors such as reactants (nature, concentration) and physical factors such as temperature and step durations. The nature of the framework sources (Al and Si sources) was found to be important because their counterions may inhibit the formation of imogolite (Farmer and Fraser, 1979). The Al to Si molar ratio is also a determinative parameter. Imogolite syntheses are usually realized in highly diluted solutions and lead to very low yields. Temperature and crystallization time are also significant parameters. The optimum temperature of crystallization

* E-mail address of corresponding author:
jocelyne.brendle@uha.fr
DOI: 10.1346/CCMN.2015.0630205

was reported to be usually <100ºC (Farmer *et al.*, 1977; Farmer and Fraser, 1979; Wada, 1987) but with long synthesis durations of up to several months. A recent study showed that larger imogolite nanotubes could be obtained with longer growth times (Levard *et al*., 2009).

A new synthesis method (Figure 1) that allows the formation of imogolite using fluoride has been reported recently (Chemmi *et al*., 2013). Imogolite nanotubes were obtained successfully with a high yield (64% *vs.* 44% in the absence of fluorine). According to powder X-ray diffraction (XRD) and ^{19}F, ^{27}Al, and ^{29}Si solid state Nuclear Magnetic Resonance (NMR), the introduction of a small amount of fluoride was found to have a positive effect on the crystallization rate.

The purpose of the present study was to assess the influences of the key parameters governing the formation of imogolite by the fluoride pathway. Seven parameters were studied: the nature of aluminum and silicon sources, the Al:Si molar ratio in the initial mixture, the amount of water used to disperse the gel collected after desalination, the F/Si molar ratio, the crystallization temperature, and time. Moreover, the role of two synthesis steps – desalination and acidification with HCl – in the formation of aluminosilicate nanotubes was also investigated. All synthesized products were studied by powder XRD, Fourier Transform Infrared spectroscopy (FTIR), and ^{19}F, ^{27}Al and ^{29}Si solid state NMR.

EXPERIMENTAL METHODS

Imogolite synthesis

In a typical synthesis procedure (Figure 1), *e.g.* from Chemmi *et al*. (2013), 200 mL of a 150 mM (or 108 mM) aqueous solution of the Al source was mixed with 200 mL of a 60 mM aqueous solution of the Si source corresponding to Al/Si ratios, R of 2.5 (or 1.8). Then, 43 mL (or 17 mL) of a 1 M NaOH solution (Sigma Aldrich Chimie S.a.r.l, Saint-Quentin Fallavier, France) was added dropwise until the pH of the solution reached 6 (OH/Al molar ratio of 1.5 or 0.8, respectively). After centrifugation ($2454 \times g$, 5810R centrifuge, Eppendorf, Montesson, France) the supernatant was removed and the white gel was washed twice with 200 mL of distilled water (desalination process). The resultant gel was dispersed in a volume, V (mL) of distilled water with V ranging from 250 mL to 2 L. At the end of the dispersion, fluorine (HF, Riedel-de-Haen AG, Buchs, Switzerland) was added (except when an inorganic fluorinated source was used) and stirred at room temperature for 10 min. The pH of the suspension, initially ~5, was lowered (or not) to 4–4.5 by adding, dropwise, aqueous 1 M HCl (Carlo Erba, Val-de-Reuil, France). The mixture was stirred for 10 min at room temperature, transferred into a closed polypropylene flask and left at a temperature T (ranging 90–98ºC) for D days (2–7). After cooling to room temperature, a limpid solution was obtained (pH = 3.5–4). An aqueous solution of ammonia (NH_4OH, 25 wt.%, Sigma Aldrich Chimie S.a.r.l, Saint-Quentin Fallavier, France) was added until the pH reached 8 leading to the formation of a gel. The solid phase was recovered by centrifugation ($2454 \times g$) and washed with distilled water (twice, in 100 mL). The gel collected was redispersed in distilled water, frozen with liquid nitrogen, and freeze-dried at −74ºC for 5 days. All the syntheses were reproduced three times and similar results were obtained.

X-ray Diffraction (XRD)

Powder XRD patterns were recorded using a PANanalytical X'PERT PRO diffractometer (PANalytical, Limeil-Brevannes, France), operating at

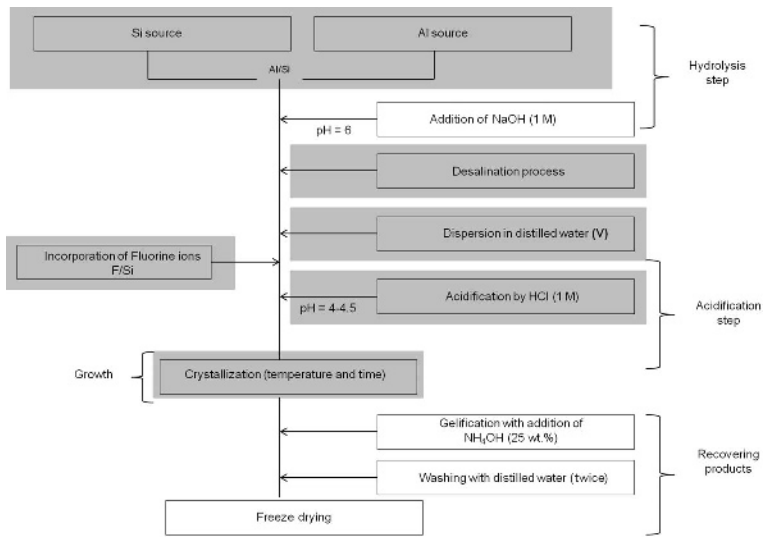

Figure 1. Schematic diagram of the synthesis protocol for the preparation of imogolite nanotubes by the fluoride route.

https://doi.org/10.1346/CCMN.2015.0630205 Published online by Cambridge University Press

a voltage of 50 kV and current of 40 mV, with CuKα radiation (1.5418 Å) produced by an excited copper anticathode and equipped with an X'Celerator real-time multiple strip detector (active length = 2.122°2θ). The powder patterns were collected at 22°C in the range 3−70°2θ (step: 0.017°2θ, time per step: 220 s).

Fourier-Transform Infrared spectroscopy (FTIR)

The FTIR spectra were recorded using a Bruker Equinox 55 spectrometer (Bruker Optics, Marne la Vallée, France). The samples were mounted as KBr pellets (1 wt.%) and the spectra were recorded routinely between 4000 and 400 cm^{-1} using a resolution of 4.0 cm^{-1} and 200 scans.

X-ray fluorescence spectroscopy (XRF)

Elemental analysis was performed by wavelength-dispersive XRF using a Philips MagiX apparatus (PANalytical, Limeil-Brevannes, France). Pellets (200 mg) were prepared under 5 tons of pressure.

Solid-state nuclear magnetic resonance spectroscopy (NMR)

^{1}H and ^{29}Si solid-state cross polarization magical angle spinning (CP-MAS) NMR spectra were recorded using a Bruker AVANCE II 300WB spectrometer (B_0 = 7.1 T) (Bruker Biospin, Wissembourg, France) operating at 59.59 MHz, with a ^{1}H pulse duration of 3.5 µs corresponding to a flip angle of π/2, a contact time of 4 ms, and a recycle delay of 4 s. Samples were packed in a 7 mm cylindrical zirconia rotor and spun at a spinning frequency of 4 kHz. The ^{27}Al and ^{19}F MAS NMR spectra were recorded using a Bruker Avance II 400 WB spectrometer (B_0 = 9.4 T) operating at 104.2 and 376.05 MHz, respectively. The ^{27}Al MAS NMR spectra were recorded using a 4 mm cylindrical zirconia rotor and spun at a spinning frequency of 14 kHz. Typical acquisition parameters were a π/12 pulse of 0.5 µs and 0.5 s of recycle delay. The ^{19}F MAS NMR spectra were recorded using a 2.5 mm cylindrical zirconia rotor, at a spinning frequency of 25 kHz. A pulse of 4 µs corresponding to a flip angle of π/2 and 30 s recycle delay were used. The chemical shifts of ^{29}Si, ^{27}Al, and ^{19}F were referenced to tetramethylsilane (TMS), an $Al(NO_3)_3$ aqueous solution, and trichloro-fluoro-methane ($CFCl_3$), respectively.

Decompositions of the NMR resonances to extract the proportions of the corresponding species were performed using the *DMfit* software (Massiot *et al.*, 2002).

Nitrogen adsorption/desorption manometry

Nitrogen adsorption/desorption isotherms were recorded at −195°C using a Micromeritics ASAP 2420 instrument (Micromeritics, Verneuil-en-Halatte, France). Prior to the measurements, the samples were outgassed at 275°C overnight under vacuum. The specific surface area (S_{BET}) was calculated according to the Brunauer-Emmett-Teller (BET) method in the range of relative pressure (p/p_0) from 0.05 to 0.12. The total pore volume (V_t) was calculated at p/p_0 of 0.98 and the microporous volume (V_m) at p/p_0 = 0.1. The pore-size distribution was evaluated with the Horvath-Kawazoe (HK) method in order to determine the internal diameter of nanotubes (Horvath and Kawazoe, 1983).

Transmission electron microscopy (TEM)

Transmission electron microscopy images were collected using a Philips CM200 microscope (Philips, Eindhoven, Netherlands) equipped with a LaB_6 filament. The accelerating voltage was 200 kV. The samples were prepared by depositing several drops of a suspension of the product in chloroform on Cu grids coated with a thin (5 nm) holey carbon film.

RESULTS AND DISCUSSION

Influence of Al sources

Imogolite syntheses were first performed according to a previous study (Chemmi *et al.*, 2013) with Na_4SiO_4 (Alfa Aesar, Schiltigheim, France) as the Si source and with three different Al sources (Al/Si = 2.5): $AlCl_3{\cdot}6H_2O$ (Fluka, Saint-Quentin Fallavier, France), $Al(NO_3)_3{\cdot}9H_2O$ (Carlo Erba, Val-de-Reuil, France) and $AlF_3{\cdot}3H_2O$ (Sigma Aldrich Chimie S.a.r.l, Saint-Quentin Fallavier, France). $Al(ClO_4)_3$ was not used due to its toxicity and reactivity. $AlF_3{\cdot}3H_2O$ was chosen to serve as the source of both Al and F (F/Si = 7.5); in this case no HF was added. For the two other Al sources, syntheses were performed by adding HF with a molar ratio F/Si of 0.1. The corresponding XRD patterns (Figure 2a) of samples obtained with $AlCl_3{\cdot}6H_2O$ and $Al(NO_3){\cdot}9H_2O$ sources are similar with four main broad reflections at 4.2°2θ (2.07 nm), 9.1°2θ (0.97 nm), 14.3°2 θ (0.61 nm), and 26.7°2 θ (0.32 nm) characteristic of the imogolite structure (Cradwick *et al.*, 1972). The most intense reflection at 4.2°2θ is attributed to the (100) plane and related to the external diameter of the nanotubes (2.07 nm). The reflection at 9.1°2θ was assigned to the (001) plane and assigned to the repetition of the structural unit of imogolite along the nanotube. These two reflections allow the imogolite structure to be confirmed (Cradwick *et al.*, 1972). The small reflection at 18.4°2θ could be attributed to the presence of gibbsite ($Al(OH)_3$, ICDD card N°: 00-001-0287), in agreement with Kleber *et al.* (2007). The formation of imogolite nanotubes was also confirmed by FTIR (Figure 2b). The spectra display bands characteristic of imogolite at 430 cm^{-1} (Al−OH stretching), 562, and 505 cm^{-1} (O−Si−O stretching), 697 cm^{-1} (O−Al−O stretching), as well as at 990 and 940 cm^{-1} (Si−O stretching vibration) (Arancibia-Miranda *et al.*, 2013; Bishop *et al.*, 2013). Note that for all samples, three additional infrared bands were also observed. The bands at 3500 cm^{-1} and 1638 cm^{-1} are assigned to OH-stretching and H_2O

https://doi.org/10.1346/CCMN.2015.0630205 Published online by Cambridge University Press

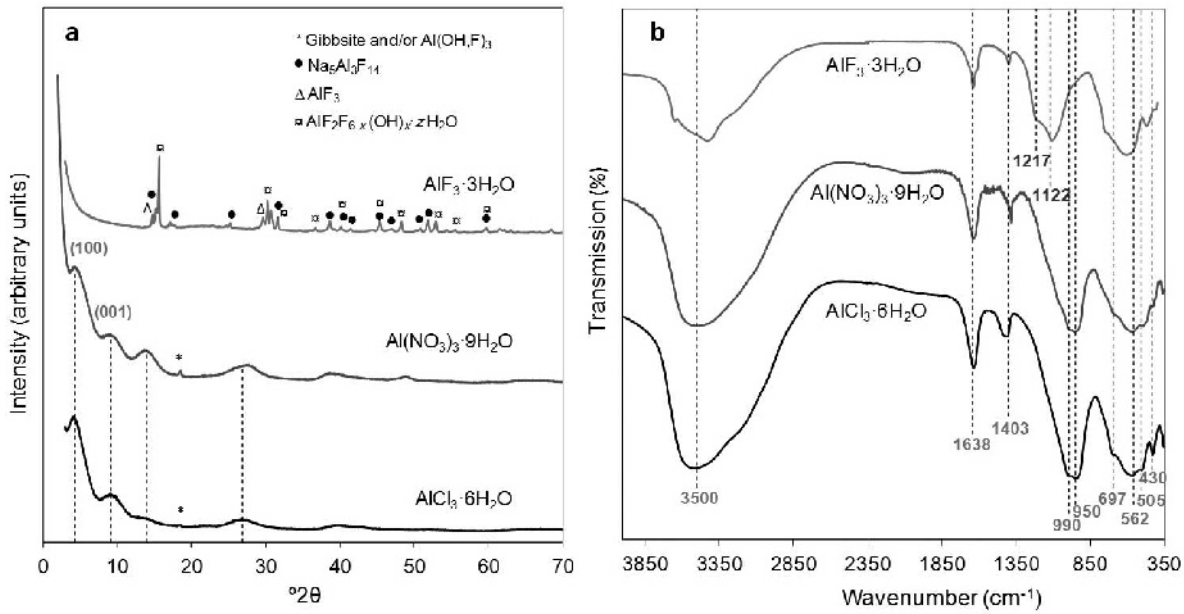

Figure 2. (a) XRD patterns (CuKα radiation) and (b) FTIR spectra of the products obtained using different Al sources: $AlCl_3{\cdot}6H_2O$, $Al(NO_3)_3{\cdot}9H_2O$, and $AlF_3{\cdot}3H_2O$.

bending modes, respectively. The band at 1403 cm^{-1} is assigned to NH_4^+ used in the flocculation step. The XRD pattern of the product obtained with $AlF_3{\cdot}3H_2O$ (Figure 2a) displays a series of peaks at 15.6°2θ (0.56 nm), 30.2°2θ (0.29 nm), 31.6°2θ (0.28 nm), 36.7°2θ (0.24 nm), 40.1°2θ (0.22 nm), 45.4°2θ (0.19 nm), 48.3°2θ (0.18 nm), 52.9°2θ (0.17 nm), 55.5°2θ (0.16 nm), and 59.7°2θ (0.15 nm). According to the International Centre for Diffraction Data (ICDD) the phase obtained corresponds to an aluminum fluoride hydroxide hydrate ($Al_2F_{6-x}(OH)_x{\cdot}zH_2O$, card N°: 00-060-0273). Other phases were also observed in the sample (Figure 2a) and attributed to sodium aluminum fluoride ($Na_4Al_3F_{14}$, card N°: 00-030-1144) and aluminum fluoride (AlF_3, card N°: 01-084-1672). A diffuse halo centered at ~23°2θ was also detected and may be due to the formation of amorphous silica. The FTIR spectrum does not present the characteristic bands of imogolite nanotubes. Instead, a broad and intense band at 1217 and 1112 cm^{-1}, characteristic of asymmetric stretching Si–O bands in an amorphous network, is observed, in agreement with XRD results (Romero *et al.*, 1997). The synthesis of imogolite nanotubes was thus successful by using $AlCl_3{\cdot}6H_2O$ or $Al(NO_3)_3{\cdot}9H_2O$ as aluminum sources. In contrast, the use of $AlF_3{\cdot}3H_2O$ did not lead to the formation of imogolite. This could be explained by the high concentration of fluorine ions in the medium (F/Si = 7.5) which appears to have favored the formation of a complex with Al leading to an aluminum fluoride hydroxide hydrate phase.

The ^{27}Al and ^{29}Si solid-state NMR experiments were performed (Figure 3) in order to study the influence of the Cl^- and NO_3^- counterions on the local environment of Si and Al in imogolite. For both samples a main ^{29}Si resonance was detected at −79 ppm consistent with the imogolite structure and corresponding to silanol groups connected to 6 Al through oxygen atoms (Barron *et al.*, 1982). Additional weak resonances between −81 and −90 ppm were observed for the sample prepared from $Al(NO_3)_3{\cdot}9H_2O$ and indicate the presence of amorphous species or defects in the imogolite structure (Figure 3, inset). Two resonances were observed in the ^{27}Al MAS NMR spectra of both samples at 4 ppm and 60 ppm corresponding to octahedral and tetrahedral aluminum, respectively (Goodman *et al.*, 1985; Wilson *et al.*, 2001). As reported in the literature (Yucelen *et al.*, 2011), the tetrahedral aluminum corresponds to poorly crystalline species or defect sites at the end of the nanotubes. Spectral decomposition revealed that the proportion of tetrahedral aluminum is negligible (2% of the total signal) when the synthesis was performed with $AlCl_3{\cdot}6H_2O$ whereas the material prepared with $Al(NO_3)_3{\cdot}9H_2O$ contains 5% tetrahedral species. Both ^{29}Si CP-MAS and ^{27}Al MAS NMR showed that the use of $AlCl_3{\cdot}6H_2O$ as an Al source produced a smaller amount of poorly crystalline species or defect sites; on this basis $AlCl_3{\cdot}6H_2O$ was selected as the Al source for further study.

Influence of Si sources

In this part, syntheses were performed with $AlCl_3{\cdot}6H_2O$ as the Al source with the same syntheses parameters as previously. In addition to Na_4SiO_4 (described in the previous section), two additional Si sources were used: $Si(OEt)_4$ (Sigma Aldrich Chimie S.a.r.l, Saint-Quentin Fallavier, France) and $FSi(OEt)_3$

https://doi.org/10.1346/CCMN.2015.0630205 Published online by Cambridge University Press

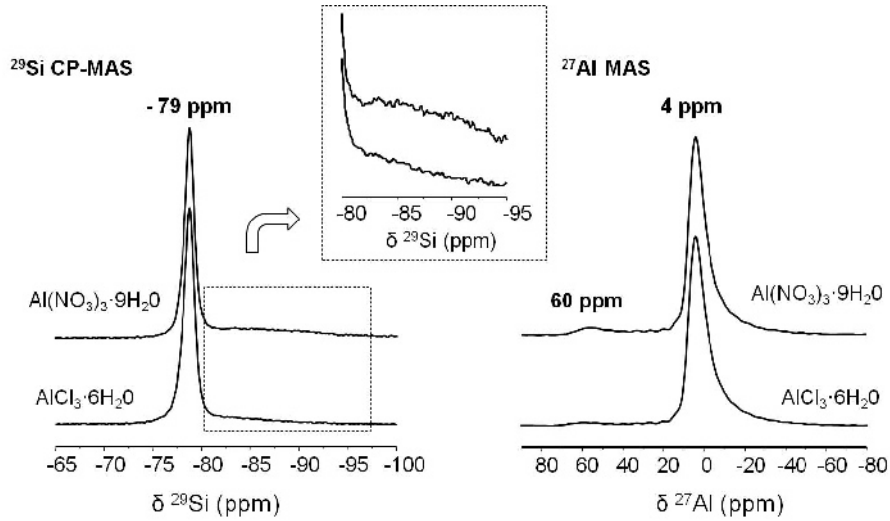

Figure 3. ^{29}Si CP-MAS and ^{27}Al MAS NMR spectra of products obtained with $AlCl_3.6H_2O$ and $Al(NO_3)_3.9H_2O$ as Al sources.

(ABCR Gmbh, Karlsruhe, Germany). $Si(OEt)_4$ is usually preferred for imogolite synthesis because of its slower condensation kinetics (Denaix *et al.*, 1999). $FSi(OEt)_3$ was selected to serve as a source of both silicon and fluorine (molar F/Si ratio = 1). The XRD patterns and FTIR spectra of the products obtained with Na_4SiO_4 and $Si(OEt)_4$ were similar and characteristic of imogolite nanotubes (Figure 4). Nevertheless, the imogolite-specific XRD reflections and FTIR bands are better defined in the Na_4SiO_4-based sample. Moreover, the FTIR spectrum (Figure 4b) of the $Si(OEt)_4$-derived sample presents a shoulder at 1070 cm^{-1} which is specific to boehmite (Priya *et al.*, 1997; Bleta *et al.*, 2011). The XRD pattern (Figure 4a) of the sample prepared with $FSi(OEt)_3$ as the source of Si and F showed six reflections at 18.4º2θ (0.48 nm), 20.4º2θ (0.43 nm), 37.0º2θ (0.24 nm), 38.2º2θ (0.23 nm), 46.3º2θ (0.19 nm), and 52.8º2θ (0.18 nm) which correspond to aluminum fluoride hydroxide ($Al(OH,F)_3$, Card Nº 00-047-1784). Thus, the possibility cannot be excluded that the small XRD peak observed previously for imogolite samples and attributed to

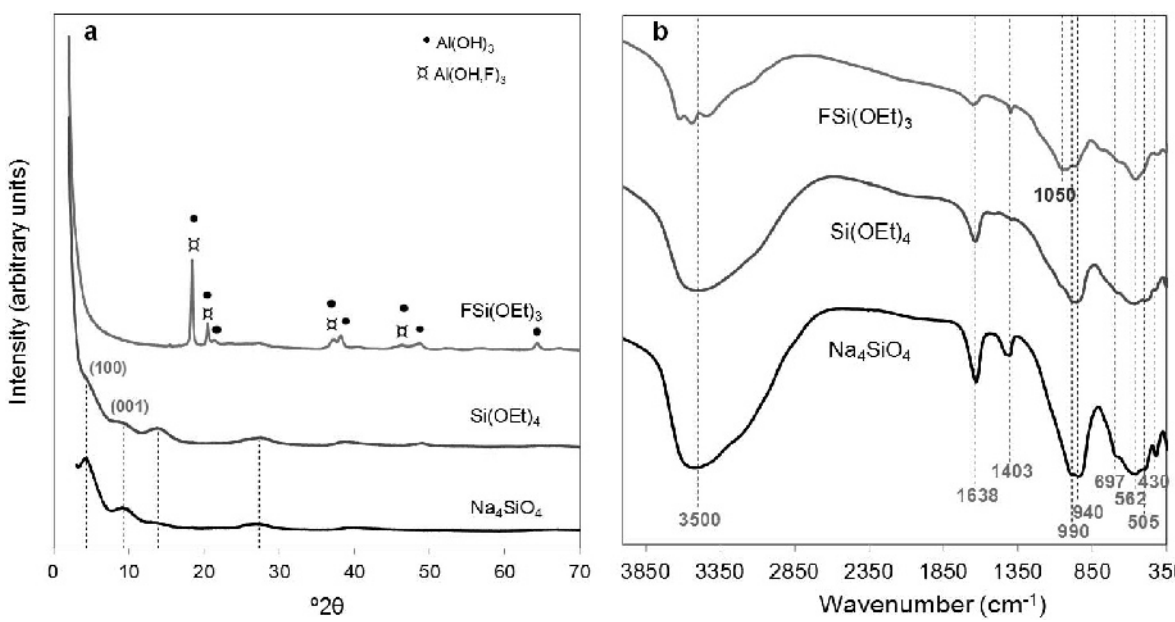

Figure 4. (a) XRD patterns (CuKα radiation) and (b) FTIR spectra of the products obtained with different Si sources: Na_4SiO_4, $Si(OEt)_4$, and $FSi(OEt)_3$.

https://doi.org/10.1346/CCMN.2015.0630205 Published online by Cambridge University Press

gibbsite (Figure 2a) was due to the formation of this $Al(OH,F)_3$ phase. Another phase that corresponds to aluminum hydroxide ($Al(OH)_3$, Card Nº 04-009-2200) was also observed (Figure 4a). $Al(OH,F)_3$ and $Al(OH)_3$ have a similar structure. A diffuse halo, weak in intensity and partly hidden by the low-angle diffraction peaks of the fluorinated gibbsite phase, was also present and probably indicates the presence of amorphous silica. The corresponding FTIR spectrum did not show the characteristic bands of imogolite nanotubes. A broad band at 1050 cm^{-1} characteristic of Si−O−Si stretching bands of amorphous silica (Umegaki *et al.*, 2014) was clearly observed. The inhibition of the formation of imogolite nanotubes by $FSi(OEt)_3$ could be explained by the excess fluorine ions (F/Si = 1) in the reaction medium, as already observed with $AlF_3{\cdot}3H_2O$. At this stage, the XRD and FTIR results favored Na_4SiO_4 as the best Si source for the synthesis of imogolite by the fluoride route.

Influence of the Al/Si molar ratio

The formation of amorphous material such as boehmite was reported by Barrett *et al.* (1991) to be favored at high Al/Si molar ratios and those authors suggested that the optimal ratio for the formation of imogolite is 1.8. In order to check whether this optimum Al/Si ratio remains the same in the presence of fluoride, synthesis was performed with $AlCl_3{\cdot}6H_2O$, Na_4SiO_4, and HF as fluoride sources. The XRD pattern of the as-prepared sample (Figure 5a) presented three broad diffraction peaks at 26.2º2θ (0.33 nm), 40.1º2θ (0.22 nm), and 66.9º2θ (0.13 nm) characteristic of amorphous material like allophane (Iyoda *et al.*, 2012). The (100) and the (001) reflections characteristic of the diameter and the fibre structure of imogolite were absent suggesting incomplete crystallization. The corresponding FTIR spectrum (Figure 5b) presented broad bands at 960 cm^{-1} and 590 cm^{-1} which correspond to the stretching of Si−O and Si−O−Al bonds in allophane (Montarges-Pelletier *et al.*, 2005). Both XRD and FTIR show that an Al/Si molar ratio of 2.5 is preferable for the formation of imogolite nanotubes by the fluoride route. Moreover, by reducing the Al/Si molar ratio from 2.5 to 1.8, another chemical parameter was also reduced: the hydrolysis ratio (OH/Al molar ratio). This parameter was demonstrated by Wada *et al.* (1979) to also influence the formation of imogolite. Nevertheless, in the present study, the influence of the hydrolysis ratio was not evaluated.

Influence of the desalination process

The desalination step aims to reduce the concentration of anions such as Cl^- which can inhibit the formation of imogolite nanotubes (Suzuki and Inukai, 2010; Kuroda *et al.*, 2012; Guimarães *et al.*, 2013). In an attempt to reduce the number of steps, synthesis was realized without this desalination process. For the sample obtained without the desalination process only four broad diffraction peaks at 14.08º2θ (0.62 nm), 26.49º2θ (0.33 nm), 39.21º2θ (0.29 nm), and 49.90º2θ (0.19 nm) specific to allophane were observed (Figure S1). The formation of allophane is also confirmed by the FTIR spectrum that presented characteristic broad bands (Figure S1 – this and other supplementary figures marked with an 'S', have been deposited with the Editor-in-Chief and are available at http://www.clays.org/JOURNAL/JournalDeposits.html). These results indicate that the desalination step is necessary for the preparation of the imogolite nanotubes by the fluoride route.

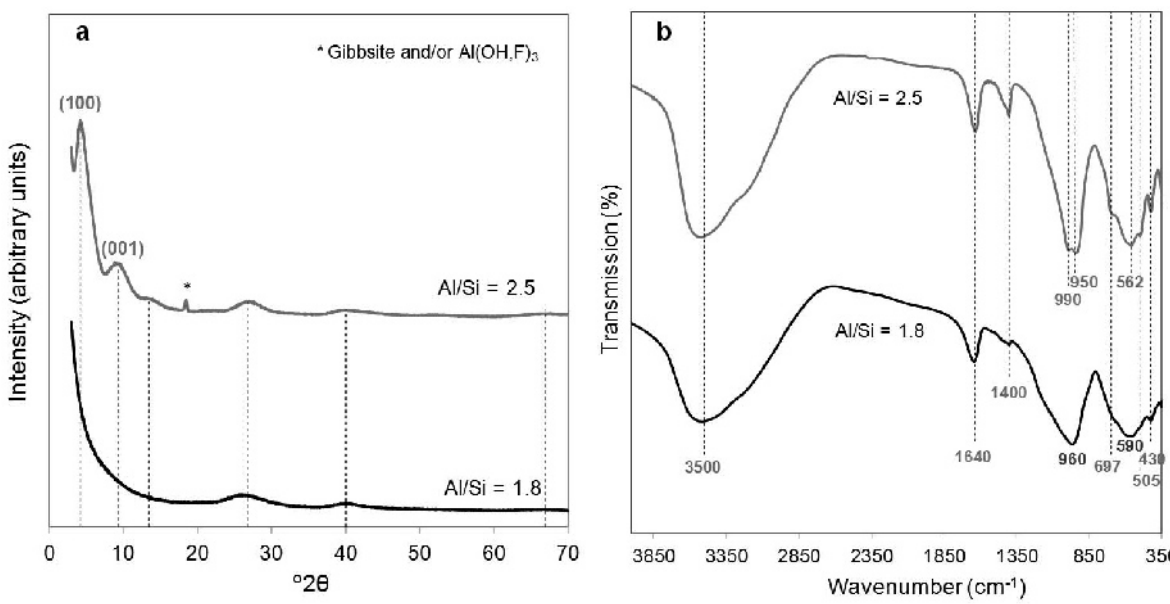

Figure 5. (a) XRD patterns and (b) FTIR spectra of samples obtained at different Al/Si molar ratios.

https://doi.org/10.1346/CCMN.2015.0630205 Published online by Cambridge University Press

Influence of the volume of H_2O used for gel dispersion after desalination

After desalination, the product was dispersed in 2 L of distilled water. To optimize the amount of distilled water used in this step, the volume was varied from 250 mL to 2 L. The XRD patterns (Figure S2) of samples obtained at low dispersion volume (between 250 and 500 mL) presented broad diffraction peaks at 14.34º2θ (0.67 nm), 26.80º2θ (0.33 nm), 39.36º2θ (0.29 nm), and 49.00º2θ (0.18 nm) which are characteristic of allophane. The allophane structure was also confirmed by FTIR (Figure S2). The XRD patterns of products prepared using larger dispersion volumes (750 mL, 1 L, and 2 L), were similar to that of imogolite nanotubes. This result was also confirmed by FTIR. The doublet band specific to the tubular structure was clearly observed at 990 and 950 cm^{-1} for samples prepared with a dispersion volume of 1 L or more. The characteristic reflections detected for samples obtained at a dispersion volume of 750 mL are less resolved than reflections observed for samples prepared using 1 or 2 L.

Samples prepared at different dispersion volumes were also characterized by ^{29}Si CP-MAS and ^{27}Al solid state MAS NMR (Figure S3). For volumes between 750 mL and 2 L, the ^{29}Si CP-MAS NMR spectra of all samples presented the main resonance at −79 ppm previously assigned to imogolite. For smaller volumes (250 and 500 mL), the ^{29}Si CP-MAS NMR spectra displayed a broader resonance at −79 ppm and a shoulder between −83 and −89 ppm assigned to less ordered silicon environments (Wilson *et al.*, 2001). The widths at half-height of the −79 ppm resonance of samples prepared at dispersion rates of 250, 500, 750 mL, and 1 and 2 L were 140, 109, 81, 76, and 70 Hz, respectively. The broadening of the resonance observed upon reducing the dispersion volume is related to a larger distribution of environment, *i.e.* bond lengths and/or bond angles, suggesting that imogolite prepared at greater dispersion volume is better organized from a local structural point of view. The ^{27}Al MAS NMR spectra of all samples showed two resonances at 4 ppm and 60 ppm corresponding to the octahedral and tetrahedral aluminum, respectively. For larger volumes, the 4 ppm resonance appeared narrower (1000 Hz instead of 1080 Hz when V = 250 mL). This suggests a better local organization, as already observed by ^{29}Si CP-MAS NMR. Moreover, the 60 ppm resonance seemed to disappear at larger volumes. According to XRD, FTIR, and NMR analyses the amount of distilled water necessary to disperse the gel collected after the desalination process can be reduced from 2 to 1 L.

Influence of the F/Si molar ratio

In most studies dealing with synthesis of clays in the presence of fluoride, the F/Si molar ratio is found to be a key factor for crystallization (Huve *et al.*, 1992). The preparation of imogolite nanotubes using the optimized conditions determined above ($AlCl_3 \cdot 6H_2O$ and Na_4SiO_4 as inorganic sources, Al/Si = 2.5, with a desalination process and 1 L of distilled water for dispersion) were carried out using various amounts of HF as the fluoride source in order to have the F/Si molar ratio ranging from 0 to 0.4. The XRD patterns of samples prepared at F/Si molar ratios of 0, 0.1, 0.2, 0.3, and 0.4 revealed clearly that the fluoride ions are necessary for the efficient formation of imogolite nanotubes under those conditions (Figure 6). The XRD pattern of the sample prepared

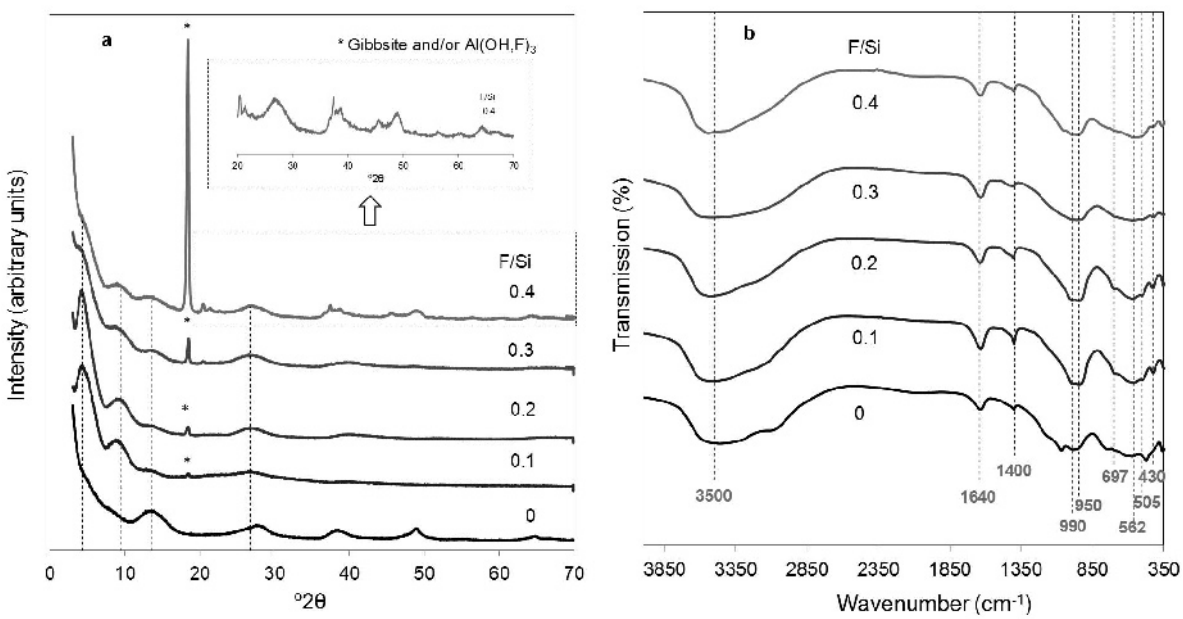

Figure 6. (a) XRD patterns (CuKα radiation) and (b) FTIR spectra of products obtained at F/Si molar ratios of 0, 0.1, 0.2, 0.3, and 0.4.

https://doi.org/10.1346/CCMN.2015.0630205 Published online by Cambridge University Press

without HF (F/Si = 0) displayed four broad peaks at 13.3º2θ (0.64 nm), 28.0º2θ (031 nm), 38.4º2θ (0.23 nm), and 49.0º2θ (0.18 nm) characteristic of allophane (Figure 6, inset), whereas the XRD patterns of samples prepared in the presence of fluorine displayed the characteristic reflections of imogolite. These reflections were, nevertheless, better defined and more intense for samples prepared with F/Si molar ratio of 0.1 and 0.2. The XRD patterns of products obtained with F/Si molar ratios of 0.3 and 0.4 presented additional intense reflections at 18.4º2θ (0.48 nm), 20.4º2θ (0.43 nm), 37.0º2θ (0.24 nm), 38.2º2θ (0.23 nm), 46.3º2θ (0.19 nm), and 52.8º2θ (0.18 nm) assigned to aluminum fluoride hydroxide ($Al(OH,F)_3$). Finally, the peak at 18.4º2θ (0.48 nm) was also observed for F/Si of 0.1 and 0.2 but with lower intensity. The FTIR data (Figure 6) were consistent with the formation of imogolite nanotubes regardless of the F/Si ratio ($\neq 0$), in agreement with XRD. Note that the infrared band doublet specific to imogolite structure at 990 and 950 cm^{-1} is clearly distinct for samples prepared with F/Si molar ratios of 0.1 and 0.2.

The local environment of F, Si, and Al atoms was studied by ^{19}F MAS, ^{29}Si CP-MAS, and ^{27}Al solid-state MAS NMR (Figure S4). The ^{29}Si CP-MAS NMR spectra of all the samples display the main resonance of imogolite at −79 ppm. At high F/Si molar ratios (0.3 and 0.4), a broad resonance at −83 ppm was observed, indicating the presence of a poorly crystallized species (protoimogolite, allophane) or structural defects (Yucelen *et al.*, 2012). The fractions of tetrahedral aluminum deduced from the decomposition of the ^{27}Al MAS NMR lines were 2, 3, 5, and 7% for products prepared with F/Si ratios of 0.1, 0.2, 0.3 and 0.4, respectively. Thus, the data from both ^{27}Al MAS and ^{29}Si CP-MAS NMR suggest that a smaller number of amorphous species or defect sites are detected when the synthesis is performed with a F/Si molar ratio of 0.1 or 0.2. These results are consistent with XRD and FTIR and confirm that at F/Si molar ratio >0.2 a mixture of imogolite nanotubes, disordered phases, and aluminum fluoride hydroxide is obtained. The samples prepared with F/Si molar ratios of 0.1 and 0.2 were analysed by ^{19}F MAS NMR and compared to fluorinated gibbsite ($Al(OH,F)_3$) (Figure 7). The low signal-to-noise ratio of the ^{19}F MAS NMR spectra of imogolite samples can be explained by the small amount of fluorine determined by X-ray fluorescence (~2 wt.% for F/Si = 0.2 and <1 wt.% for F/Si = 0.1). The ^{19}F MAS NMR spectrum of $(Al(OH,F)_3$ showed one broad component at −134 ppm. For samples prepared with F/Si molar ratios of 0.1 and 0.2, at least 3 and 2 resonances, respectively, were observed in the −115 to −155 ppm range. This suggests that these resonances could be partly assigned to fluorinated gibbsite. At this stage it is difficult to differentiate the fluorine of fluorinated gibbsite and the fluorine incorporated into the imogolite structure. In conclusion, the preparation of imogolite nanotubes requires fine control of the F/Si ratio; in fluorine-free conditions or in a highly fluorinated medium the formation of other phases is favored.

Influence of the acidification process

The influence of the acidification step on the formation of imogolite using the fluoride route was also studied. Before the addition of HF solution to the reaction medium, the pH of the dispersed gel was 5. After the addition of HF, the pH of the reaction medium decreased to 4.5. In classical imogolite synthesis protocols (Mukherjee *et al*., 2005), the acidification step consists of decreasing the pH to a value between 5 and 4. Consequently, the pH of the solution measured after the addition of HF is in the required pH range without any addition of HCl. This suggests that the HCl acidification step could be removed from the synthesis procedure. A synthesis was performed by the fluoride route (F/Si = 0.2) without the addition of HCl. The XRD patterns (Figure S5) displayed the four broad diffraction peaks characteristic of imogolite as well as an additional sharp reflection at 18.4º2θ (0.48 nm) characteristic of fluorinated aluminum-hydroxide. The FTIR spectrum also displayed the specific bands of imogolite (Figure S5).

The local environment of Si atoms was investigated by ^{29}Si solid-state NMR (Figure S6). For both samples the main imogolite resonance at −79 ppm was detected

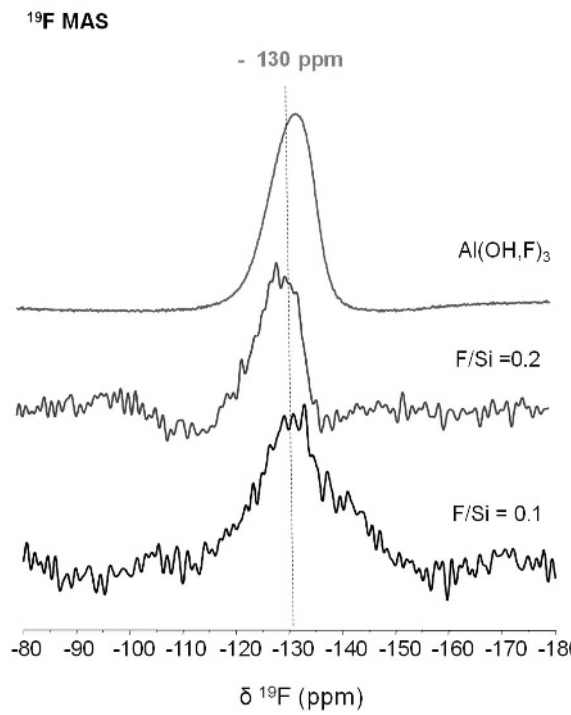

Figure 7. ^{19}F MAS NMR spectra of fluorinated gibbsite ($Al(OH,F)_3$) and samples obtained at molar ratios of F/Si = 0.1 and 0.2.

https://doi.org/10.1346/CCMN.2015.0630205 Published online by Cambridge University Press

in agreement with XRD and FTIR results. Nevertheless, a broad shoulder at −83 ppm was detected for the sample prepared in the absence of HCl solution suggesting the presence of a less ordered silicon environment. As a result, the HCl acidification step improves the formation of well organized imogolite nanotubes.

Influence of crystallization temperature and time

The temperature of crystallization was varied from 90 to 98ºC with a crystallization time of 7 days. All samples displayed similar XRD patterns (Figure S7) showing the four broad reflections of imogolite. The reflections observed in XRD patterns of samples prepared at 95 and 98ºC were better defined than those of the samples prepared at 90ºC. The FTIR spectra confirmed that imogolite was formed regardless of the growth temperature (Figure S7). In agreement with the findings of XRD, the bands characteristic of imogolite are broader with a crystallization temperature of 90ºC. Both XRD and FTIR data suggest the formation of better-crystallized imogolite nanotubes at 95 and 98ºC. The ^{29}Si CP-MAS and ^{27}Al MAS NMR spectra of the sample prepared at 90ºC confirm this result (Figure S8). The fraction of Al in tetrahedral coordination determined by ^{27}Al MAS NMR was ~1% instead of 3% when the synthesis was performed at 95ºC and 90ºC, respectively, and negligible (<1%) when the synthesis was performed at 98ºC. According to these results, the optimum crystallization temperature leading to a well organized imogolite is 98ºC.

The influence of the growth time was also investigated by varying the duration of the crystallization step from 2 to 7 days with the above conditions ($AlCl_3{\cdot}6H_2O$ and Na_4SiO_4 as inorganic sources, desalination step, 1 L of H_2O for gel redispersion, HF (F/Si = 0.2), acidification step, and crystallization temperature of 98ºC). Crystallization times ranging from 3 to 7 days resulted in similar XRD patterns (Figure S9) characteristic of imogolite. The XRD pattern of the sample prepared with a crystallization time of 2 days was clearly different and displayed broad reflections corresponding to amorphous species such as allophane. This observation was confirmed by the FTIR spectra (Figure S9). The IR bands of imogolite observed after a 3-day growth time are broader than those observed for a growth time of 4 days. Furthermore, a shoulder at 1141 cm^{-1} was also observed, revealing the presence of boehmite. Imogolite nanotubes are better structured when the synthesis is performed with a crystallization time of >4 days. This was also confirmed by ^{29}Si CP-MAS and ^{27}Al MAS NMR (Figure S10). The samples prepared with crystallization times of 2 and 3 days also presented similar, small fractions of tetrahedral aluminum (2%) instead of 6% for the other samples. Overall, the growth time of imogolite can be reduced from 7 to 4 days, but the yield decreased from 80 to 55%.

Morphology and textural properties

Synthetic imogolite prepared by the aforementioned optimized synthetic route was further analyzed by TEM and nitrogen adsorption/desorption. The sample consists of entangled fibrous bundles forming a web-like network (Figure 8). The bundles are similar to those observed for imogolite prepared by classical synthesis protocols (Koenderink *et al*., 1999; Mukherjee *et al*., 2005).

A Type IV N_2 adsorption/desorption isotherm with hysteresis loops indicating the presence of mesopores was observed (Figure 9). The steep increase at low relative pressure (p/p_0) indicates the presence of micropores. The specific surface area (S_{BET}), evaluated using the BET equation, was 330 m^2g^{-1}. The total volume (V_t), measured at p/p_0 of 0.98 was 0.22 $cm^3\ g^{-1}$ and the micropore volume (V_m) measured at p/p_0 of 0.1 was 0.12 $cm^3\ g^{-1}$. The pore-size distribution calculated by the Horvath-Kawazoe (HK) method showed a maximum centered at 1.2 nm (Figure 9). These values are in agreement with previous results described by Adams (1980).

CONCLUSION

The fluoride route was applied successfully to the preparation of imogolite nanotubes. The influence of several chemical and physical parameters was investigated. Both XRD and FTIR were used to check the formation of imogolite. ^{29}Si and ^{27}Al solid-state NMR was found to be a powerful tool for gathering information about the local environment of Si and Al nuclei, in particular in relation to the presence of structural defects. Well crystallized imogolite nanotubes (55%

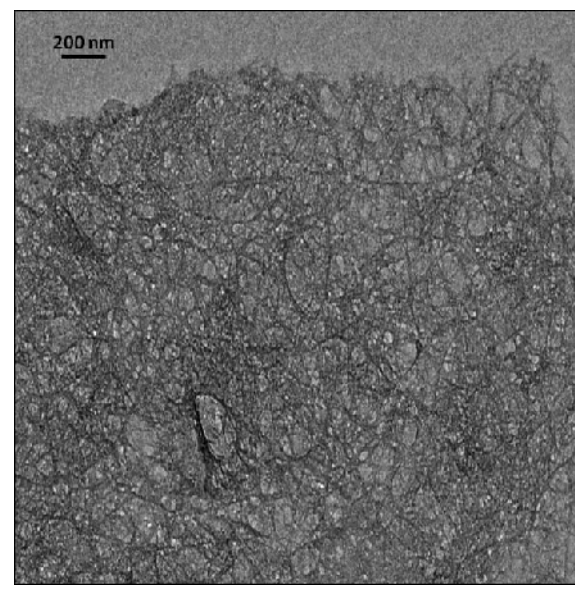

Figure 8. TEM image of freeze-dried synthetic imogolite.

https://doi.org/10.1346/CCMN.2015.0630205 Published online by Cambridge University Press

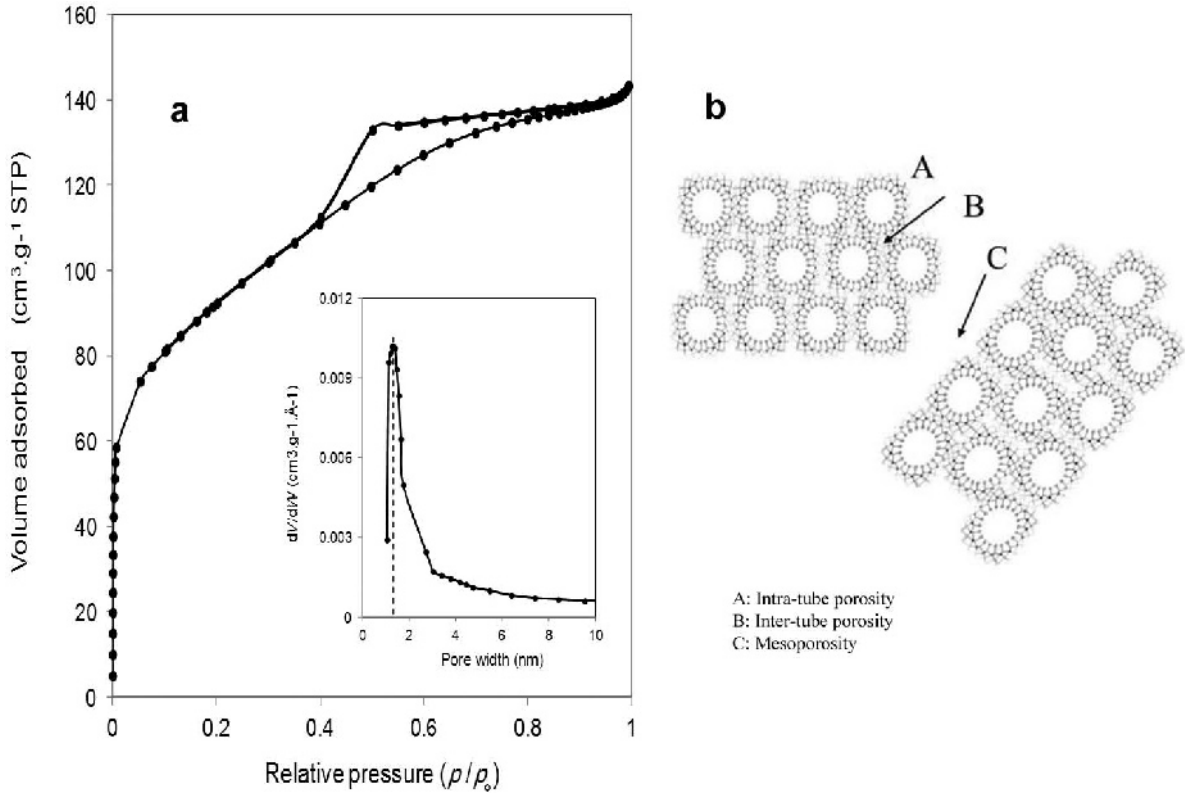

Figure 9. Nitrogen adsorption/desorption isotherm and HK pore-size distribution of imogolite prepared in the presence of fluorine.

yield) can be obtained with a minimum of unwanted species by using $AlCl_3 \cdot 6H_2O$ and Na_4SiO_4 as Al and Si sources, respectively, with an Al/Si molar ratio of 2.5, in the presence of HF as the source of F, with a F/Si molar ratio of 0.1 or 0.2, a crystallization temperature of 98ºC, and a crystallization time of at least 4 days. A lack of fluorine favors the formation of allophane, whereas an excess of fluorine leads to the formation of a fluorinated aluminum hydroxide-like phase. Studies are underway in order to check the influence of the Al/OH molar ratio and to determine the role of the different parameters on the length of the imogolite nanotubes.

REFERENCES

Ackerman, W.C., Smith, D.M., Huling, J.C., Kim, Y.W., Bailey, J.K., and Brinker, C.J. (1993) Gas/vapor adsorption in imogolite: a microporous tubular aluminosilicate. *Langmuir*, **9**, 1051–1057.

Adams, J.M. (1980) Gas chromatographic adsorption studies on synthetic imogolite. *Journal of Chromatography A*, **188**, 97–106.

Arancibia-Miranda, N., Escudey, M., Molina, M., and García-González, M. (2013) Kinetic and surface study of single-walled aluminosilicate nanotubes and their precursors. *Nanomaterials*, **3**, 126–140.

Barrett, S.M., Budd, P.M., and Price, C. (1991) The synthesis and characterization of imogolite. *European Polymer Journal*, **27**, 609–612.

Barron, P.F., Wilson, M.A., Campbell, A.S., and Frost, R.L. (1982) Detection of imogolite in soils using solid state ^{29}Si NMR. *Nature*, **299**, 616–618.

Bishop, J.L., Rampe, E.B., Bish, D.L., Abidin, Z.L., Baker, L.L., Matsue, N., and Henmi, T. (2013) Spectral and hydration properties of allophane and imogolite. *Clays and Clay Minerals*, **61**, 57–74.

Bleta, R., Jaubert, O., Gressier, M., and Menu, M.-J. (2011) Rheological behaviour and spectroscopic investigations of cerium-modified AlO(OH) colloidal suspensions. *Journal of Colloid and Interface Science*, **363**, 557–565.

Chemmi, A., Brendlé, J., Marichal, C., and Lebeau, B. (2013) A novel fluoride route for the synthesis of aluminosilicate nanotubes. *Nanomaterials*, **3**, 117–125.

Clark, C.J. (1984) Chemisorption of Cu(II) and Co(II) on allophane and imogolite. *Clays and Clay Minerals*, **32**, 300–310.

Cradwick, P.C.G., Farmer, V.C., Russell, J.D., Masson, C.R., Wada, K., and Yoshinaga, N. (1972) Imogolite, a hydrated aluminium silicate of tubular structure. *Nature Physical Science*, **240**, 187–189.

Denaix, L., Lamy, I., and Bottero, J.Y. (1999) Structure and affinity towards Cd^{2+}, Cu^{2+}, Pb^{2+} of synthetic colloidal amorphous aluminosilicates and their precursors. *Colloids and Surfaces A: Physicochemical and Engineering Aspects*, **158**, 315–325.

Farmer, V.C. (1983) Synthetic imogolite: Properties, synthesis, and possible applications. *Clay Minerals*, **18**, 459–472.

Farmer, V.C. and Fraser, A.R. (1979) Synthetic imogolite, a tubular hydroxyaluminium silicate. Pp. 547–553 in: *Proceedings of the VI International Clay Conference, Oxford, UK* (M.M. Mortland and V.C. Farmer, editors). Developments in Sedimentology, **27**. Elsevier, Amsterdam.

https://doi.org/10.1346/CCMN.2015.0630205 Published online by Cambridge University Press

Farmer, V.C., Fraser, A.R., and Tait, J.M. (1977) Synthesis of imogolite: a tubular aluminium silicate polymer. *Journal of the Chemical Society, Clinical Communications*, **12**, 462–463.

Goodman, B.A., Russell, J.D., Montez, B., Oldfield, E., and Kirkpatrick, R.J. (1985) Structural studies of imogolite and allophanes by aluminum-27 and silicon-29 nuclear magnetic resonance spectroscopy. *Physics and Chemistry of Minerals*, **12**, 342–346.

Guimarães, L., Pinto, Y.N., Lourenço, M.P., and Duarte, H.A. (2013) Imogolite-like nanotubes: structure, stability, electronic and mechanical properties of the phosphorous and arsenic derivatives. *Physical Chemistry Chemical Physics*, **15**, 4303–4309.

Gustafsson, J.P. (2001) The surface chemistry of imogolite. *Clays and Clay Minerals*, **49**, 73–80.

Hongo, T., Sugiyama, J., Yamazaki, A., and Yamasaki, A. (2013) Synthesis of imogolite from rice husk ash and evaluation of its acetaldehyde adsorption ability. *Industrial & Engineering Chemistry Research*, **52**, 2111–2115.

Horvath, G. and Kawazoe, K. (1983) Method for the calculation of effective pore size distribution in molecular sieve carbon. *Journal of Chemical Engineering of Japan*, **16**, 470–475.

Hu, J., Kamali Kannangara, G.S., Wilson, M.A., and Reddy, N. (2004) The fused silicate route to protoimogolite and imogolite. *Journal of Non-Crystalline Solids*, **347**, 224–230.

Huve, L., Delmotte, L., Martin, P., Dred, R., Le Baron, J., and Saehr, D. (1992) ^{19}F MAS-NMR study of structural fluorine in some natural and synthetic 2:1 layer silicates. *Clays and Clay Minerals*, **40**, 186–191.

Imamura, S., Kokubu, T., Yamashita, T., Okamoto, Y., Kajiwara, K., and Kanai, H. (1996) Shape-selective copper-loaded imogolite catalyst. *Journal of Catalysis*, **160**, 137–139.

Iyoda, F., Hayashi, S., Arakawa, S., John, B., Okamoto, M., Hayashi, H., and Yuan, G. (2012) Synthesis and adsorption characteristics of hollow spherical allophane nano-particles. *Applied Clay Science*, **56**, 77–83.

Jiravanichanun, N., Yamamoto, K., Irie, A., Otsuka, H., and Takahara, A. (2009) Preparation of hybrid films of aluminosilicate nanofiber and conjugated polymer. *Synthetic Metals*, **159**, 885–888.

Johnson, L.M. and Pinnavaia, T.J. (1990) Silylation of a tubular aluminosilicate polymer (imogolite) by reaction with hydrolyzed (γ-aminopropyl)triethoxysilane. *Langmuir*, **6**, 307–311.

Kleber, M., Schwendenmann, L., Veldkamp, E., Röβner, J., and Jahn, R. (2007) Halloysite versus gibbsite: Silicon cycling as a pedogenetic process in two lowland neotropical rain forest soils of La Selva, Costa Rica. *Geoderma*, **138**, 1–11.

Koenderink, G.H., Kluijtmans, S.G.J., and Philipse, A.P. (1999) On the synthesis of colloidal imogolite fibers. *Journal of Colloid and Interface Science*, **216**, 429–431.

Kuroda, Y., Fukumoto, K., and Kuroda, K. (2012) Uniform and high dispersion of gold nanoparticles on imogolite nanotubes and assembly into morphologically controlled materials. *Applied Clay Science*, **55**, 10–17.

Levard, C., Rose, J., Masion, A., Doelsch, E., Borschneck, D., Olivi, L., Dominici, C., Grauby, O., Woicik, J.C., and Bottero, J.-Y. (2008) Synthesis of large quantities of single-walled aluminogermanate nanotube. *Journal of the American Chemical Society*, **130**, 5862–5863.

Levard, C., Masion, A., Rose, J., Doelsch, E., Borschneck, D., Dominici, C., Ziarelli, F., and Bottero, J.-Y. (2009) Synthesis of imogolite fibers from decimolar concentration at low temperature and ambient pressure: A promising route for inexpensive nanotubes. *Journal of the American Chemical Society*, **131**, 17080–17081.

Ma, W., Otsuka, H., and Takahara, A. (2011) Preparation and properties of PVC/PMMA-g-imogolite nanohybrid via surface-initiated radical polymerization. *Polymer*, **52**, 5543–5550.

Massiot, D., Fayon, F., Capron, M., King, I., Calv, S. Le, Alonso, B., Durand, J.-O., Bujoli, B., Gan, Z., and Hoatson, G. (2002) Modelling one- and two-dimensional solid-state NMR spectra. *Magnetic Resonance in Chemistry*, **40**, 70–76.

Montarges-Pelletier, E., Bogenez, S., Pelletier, M., Razafitianamaharavo, A., Ghanbaja, J., Lartiges, B., and Michot, L. (2005) Synthetic allophane-like particles: textural properties. *Colloids and Surfaces A: Physicochemical and Engineering Aspects*, **255**, 1–10.

Mukherjee, S., Bartlow, V.M., and Nair, S. (2005) Phenomenology of the growth of single-walled aluminosilicate and aluminogermanate nanotubes of precise dimensions. *Chemistry of Materials*, **17**, 4900–4909.

Mukherjee, S., Kim, K., and Nair, S. (2007) Short, highly ordered, single-walled mixed-oxide nanotubes assembled from amorphous nanoparticles. *Journal of the American Chemical Society*, **129**, 6820–6826.

Ohashi, F., Tomura, S., Akaku, K., Hayashi, S., and Wada, S.-I. (2004) Characterization of synthetic imogolite nanotubes as gas storage. *Journal of Materials Science*, **39**, 1799–1801.

Priya, G.K., Padmaja, P., Warrier, K.G.K., Damodaran, A.D., and Aruldhas, G. (1997) Dehydroxylation and high temperature phase formation in sol-gel boehmite characterized by Fourier transform infrared spectroscopy. *Journal of Materials Science Letters*, **16**, 1584–1587.

Romero, A.A., Alba, M.D., Zhou, W., and Klinowski, J. (1997) Synthesis and characterization of the mesoporous silicate molecular sieve MCM-48. *The Journal of Physical Chemistry B*, **101**, 5294–5300.

Suzuki, M. and Inukai, K. (2010) Synthesis and applications of imogolite nanotubes. Pp. 159–167 in: *Inorganic and Metallic Nanotubular Materials* (T. Kijima, editor). Topics in Applied Physics, **27**, Springer, Berlin.

Theng, B.K.G., Russell, M., Churchman, G.J., and Parfitt, R.L. (1982) Surface properties of allophane, halloysite, imogolite. *Clays and Clay Minerals*, **30**, 143–149.

Thomas, B., Coradin, T., Laurent, G., Valentin, R., Mouloungui, Z., Babonneau, F., and Baccile, N. (2012) Biosurfactant-mediated one-step synthesis of hydrophobic functional imogolite nanotubes. *RSC Advances*, **2**, 426–435.

Umegaki, T., Hosoya, T., Toyama, N., Xu, Q., and Kojima, Y. (2014) Fabrication of hollow silica–zirconia composite spheres and their activity for hydrolytic dehydrogenation of ammonia borane. *Journal of Alloys and Compounds*, **608**, 261–265.

Wada, S.-I. (1987) Imogolite synthesis at 25ºC. *Clays and Clay Minerals*, **35**, 379–384.

Wada, S.-I., Eto, A., and Wada, K. (1979) Synthetic allophane and imogolite. *Journal of Soil Science*, **30**, 347–355.

Wilson, M.A., Lee, G.S., and Taylor, R.C. (2001) Tetrahedral rehydration during imogolite formation. *Journal of Non-Crystalline Solids*, **296**, 172–181.

Wilson, M.A., Lee, G.S.H., and Taylor, R.C. (2002) Benzene displacement on imogolite. *Clays and Clay Minerals*, **50**, 348–351.

Yamamoto, K., Otsuka, H., Takahara, A., and Wada, S.-I. (2002) Preparation of a novel (polymer/inorganic nanofiber) composite through surface modification of natural aluminosilicate nanofiber. *The Journal of Adhesion*, **78**, 591–602.

Yoshinaga, N. and Aomine, S. (1962) Imogolite in some ando soils. *Soil Science and Plant Nutrition*, **8**, 22–29.

Yucelen, G.I., Choudhury, R.P., Leisen, J., Nair, S., and

Beckham, H.W. (2012) Defect structures in aluminosilicate single-walled nanotubes: A solid-state nuclear magnetic resonance investigation. *The Journal of Physical Chemistry C*, **116**, 17149–17157.

Yucelen, G.I., Choudhury, R.P., Vyalikh, A., Scheler, U., Beckham, H.W., and Nair, S. (2011) Formation of single-walled aluminosilicate nanotubes from molecular precursors and curved nanoscale intermediates. *Journal of American Chemical Society*, **133**, 5397–5412.

Zanzottera, C., Armandi, M., Esposito, S., Garrone, E., and Bonelli, B. (2012) CO_2 adsorption on aluminosilicate single-walled nanotubes of imogolite type. *The Journal of the Physical Chemistry C*, **116**, 20417–20425.

(*Received 22 September 2014; revised 8 April 2015; Ms 916; AE: G. Chryssikos*)